

## Article

# Construction of Geosynthetic–Reinforced Pavements and Evaluation of Their Impacts

Danrong Wang <sup>1,\*</sup> , Sheng-Lin Wang <sup>1</sup> , Susan Tighe <sup>2</sup>, Sam Bhat <sup>3</sup> and Shunde Yin <sup>1,\*</sup>

<sup>1</sup> Department of Civil and Environmental Engineering, University of Waterloo, Waterloo, ON N2L 3G1, Canada; s545wang@uwaterloo.ca

<sup>2</sup> Department of Civil Engineering, McMaster University, Hamilton, ON L8S 4L8, Canada; tighes1@mcmaster.ca

<sup>3</sup> Titan Environmental Containment Ltd., Ile des Chenes, MB R0A 0T1, Canada; sam@titanenviro.ca

\* Correspondence: peggie.wang@uwaterloo.ca (D.W.); shunde.yin@uwaterloo.ca (S.Y.)

**Abstract:** Geosynthetic materials (i.e., geogrids, geotextiles and other geocomposites) act as an inter-layer system and are widely used in construction applications. In pavement structures, geosynthetic layers provide potential benefits such as reinforcement, reflective cracking mitigation, increased fatigue life, and improved drainage and filtering. However, few studies have addressed the installation and construction practices of geosynthetics in pavements. Furthermore, the study of geosynthetics and their contribution during construction are limited. In this paper, a full-scale field study was conducted and three trial sections were constructed; two types of geosynthetics, a fibreglass geogrid and a geogrid composite, were installed in the asphalt binder course and at the interface between the subgrade and base layer, respectively, to be compared with a control section without geosynthetic reinforcement. Trial sections were instrumented to monitor the pressure applied on the subgrade, the strain in the base lift of the asphalt binder course, the temperature, and the moisture within the pavement structure during construction. In addition, post-construction field testing was performed to measure the stiffness of the pavements after construction. The results indicated that geosynthetic-reinforced pavements can maintain pavement resilience during construction and significantly mitigate the disturbances caused by construction activities. The geogrid embedded in the asphalt layer was demonstrated to reduce the pressure at the subgrade caused by paving equipment by 70% compared with the control section, while simultaneously reducing the longitudinal and transverse strain at the bottom of the asphalt layer by 54% and 99%. Observations from the geogrid composite test section also demonstrate the potential to minimize the impacts of future freeze–thaw at the subgrade due to the improved drainage and indirect insulation effect.

**Keywords:** geosynthetics; fibreglass geogrid; geogrid composite; pavement; roads; full-scale tests; construction



**Citation:** Wang, D.; Wang, S.-L.; Tighe, S.; Bhat, S.; Yin, S.

Construction of Geosynthetic–Reinforced Pavements and Evaluation of Their Impacts. *Appl. Sci.* **2023**, *13*, 10327. <https://doi.org/10.3390/app131810327>

Academic Editor: Luis Picado Santos

Received: 18 August 2023

Revised: 11 September 2023

Accepted: 13 September 2023

Published: 15 September 2023



**Copyright:** © 2023 by the authors. Licensee MDPI, Basel, Switzerland. This article is an open access article distributed under the terms and conditions of the Creative Commons Attribution (CC BY) license (<https://creativecommons.org/licenses/by/4.0/>).

## 1. Introduction

Frost and thaw actions are one of the major causes of deterioration in pavement structures undergoing freeze–thaw cycles. As such, it is necessary to investigate useful and cost-effective techniques to mitigate freeze–thaw disturbances. Commonly, geosynthetic interlayers are one option that can provide reinforcement, separation, and filtration to pavements. Furthermore, geosynthetics can be used to mitigate freeze–thaw disturbances by minimizing the frost heaves and thaw settlements; they are also adaptable to many climates, easy to install, and cost-efficient.

Geogrids are typically made by extruding Polyethylene or Polypropylene filaments or by weaving Polyester ribs into grid-like materials with openings [1]. Typically, there are three types of geogrids with uniaxial, biaxial, and triaxial grids offering reinforcement in one, two, or three directions, respectively. Geogrids have been widely used in civil engineering applications, such as in brick structures to mitigate the impact of seismic

activity [2], in pile-supported deep foundation structures to enhance their resilience [3], to reinforce and stabilize soils on slopes for building construction [4], and to reinforce weak subgrade materials in railway construction [5]. Geogrids are also widely applied in pavement structures as they can greatly strengthen an asphalt layer and mitigate reflective cracking. When placed between asphalt layers, the geogrid can function as a tensile element redirecting a crack horizontally along the interlayer [6]. The open apertures can also provide interlocking and effective bonding with the asphalt particles. Laboratory testing by Brown et al. (2001) was used to create a theoretical model to study the mitigation of reflective cracking of geogrid in an asphalt layer [7]. A similar study used finite element modelling to investigate the Von Mises stresses in the geosynthetics-reinforced asphalt concrete layer [8]. The fatigue resistance of prismatic asphalt beams with and without geogrid reinforcement was also investigated by Lee (2008), where it was demonstrated that geogrid-reinforced specimens exhibited significantly greater fatigue resistance compared to unreinforced control specimens [9]. Lee (2008) also reported that the rate of upward crack propagation was decreased by the geogrid. Similar performance improvements were also observed in the study by Arsenie et al. (2016), which used finite element modelling to demonstrate that the fatigue life of asphalt concrete could be increased with geogrid reinforcement [10]. Laboratory testing was also performed to verify the capability of geogrid to enhance the fatigue resistance of asphalt concrete by bending tests [11] as well as flexural testing combined with digital image correlation techniques [10–12]. Li et al. (2022) also found that the cracking resistance of asphalt specimens was enhanced by the installation of a geogrid interlayer when undergoing fatigue testing at lower temperatures [13].

A geogrid composite (i.e., a geogrid bonded to a geotextile) has the combined functions of separation, filtration, and drainage provided by the geotextile and reinforcement provided by the geogrid. These composites are more commonly used for weak subgrade and frost-susceptible soils. The usage of geogrid composites has been demonstrated to reduce stresses within the subgrade [14] as well as to save construction costs through the reduction of the granular base thickness [15]. Large-scale field tests have demonstrated that rutting depths are significantly reduced with reinforcement at the base and subbase interfaces [16]. A long-term field trial conducted by Aran (2006) from 1991 to 2005 demonstrated that the overall thickness of the base asphalt layer could be reduced when incorporating geogrid at the middle of the base layers, allowing for materials savings and with similar performance to the control sections [17]. Geogrids have also been tested in the base layer and base subgrade interfaces, demonstrating a notable reduction in rutting depth and permanent deformation [18]. In a subsequent study on the same trial section, it was demonstrated that at least a 20% reduction in rutting depth could be provided by installing geogrid at the interface of the base and subgrade [19]. A further review of full-scale studies using geosynthetic-reinforced flexible pavements found that they could reduce vertical deformation and delay rutting [20].

When used in pavement rehabilitation, geogrids placed underneath asphalt overlays were shown to reduce rutting in the surface course [21]. Trials on the Qinghai–Tibet highway demonstrated that the drainage effect of geotextiles also reduced the frost penetration and thaw depth, thus preserving the underlying permafrost and minimizing further thaw [22]. This structure was better suited to prevent moisture flow from soil to the gravel layer and provide better drainage effects. Tingle and Webster (2003) conducted a full-scale test on an unpaved road with geogrids laid over non-woven geotextiles embedded at the interface of granular base and subgrade layers; the outcomes of this study were used to supplement the design of unpaved roads for the United States Army Corps of Engineers [23]. A field trial with geocomposite serving as an interlayer treatment was evaluated by testing cored samples in the laboratory using an interlayer shear test [24].

In general, it can be deduced that the proper installation of geosynthetics is crucial, and improper placement could affect the post-construction evaluation of the resilience of the materials [25,26]. Nevertheless, there are limited studies examining the performance of geosynthetic-reinforced pavements in the real world and with full-scale studies. Asphalt

layers with geogrid reinforcement are rarely discussed in the context of full-scale field studies, and are even less commonly studied with sophisticated instrumentation and sensors to monitor the actual pavement response during geogrid installation. Limited research has been conducted on geogrid composites during installation thus the impacts of these interlayer systems under construction are still unexplored. In this paper, a practical field study regarding the instrumentation of geosynthetic-reinforced pavements was presented; the installation of both geosynthetics and sensors is introduced, and the effect of these interlayer systems is investigated during construction. In this large-scale study, geogrid reinforced asphalt and geogrid composite on the subgrade were investigated in real-time using pressure, strain temperature, and moisture instrumentation. Post-construction deflection measurements were conducted to verify instrument readings and demonstrate the resultant benefits of these interlayer systems.

## 2. Field Construction

### 2.1. Overview

The project site is located on Snyder Road East, Baden, Ontario. The test section is 45 m in length in total, composed of three trial sections that are each 15 m long. As shown in Figure 1, the pavement structure was composed of a 200 mm thick asphalt concrete layer and a 450 mm thick granular base layer, underlain by the subgrade. The asphalt concrete layer is composed of one lift of 50 mm surface course using a Superpave (SP) 12.5 asphalt mixture compacted over two 75 mm binder course lifts using an SP 19 asphalt mixture. The “12.5” and “19” in the designations of the asphalt mixtures refer to the maximum aggregate size (MAS), which are 12.5 mm and 19 mm, respectively. These mixes are commonly used in pavement design standards in Southern Ontario [27]. The base for all three sections is composed of an unbounded granular layer [28]. The pavement structural design is based on an Average Annual Daily Traffic (AADT) of 9573 and cumulative Equivalent Single Axle Loading (ESAL) of 3,608,000 ESALs with 5% trucks, 2% growth rate, and 20 MPa estimated resilient modulus [29].

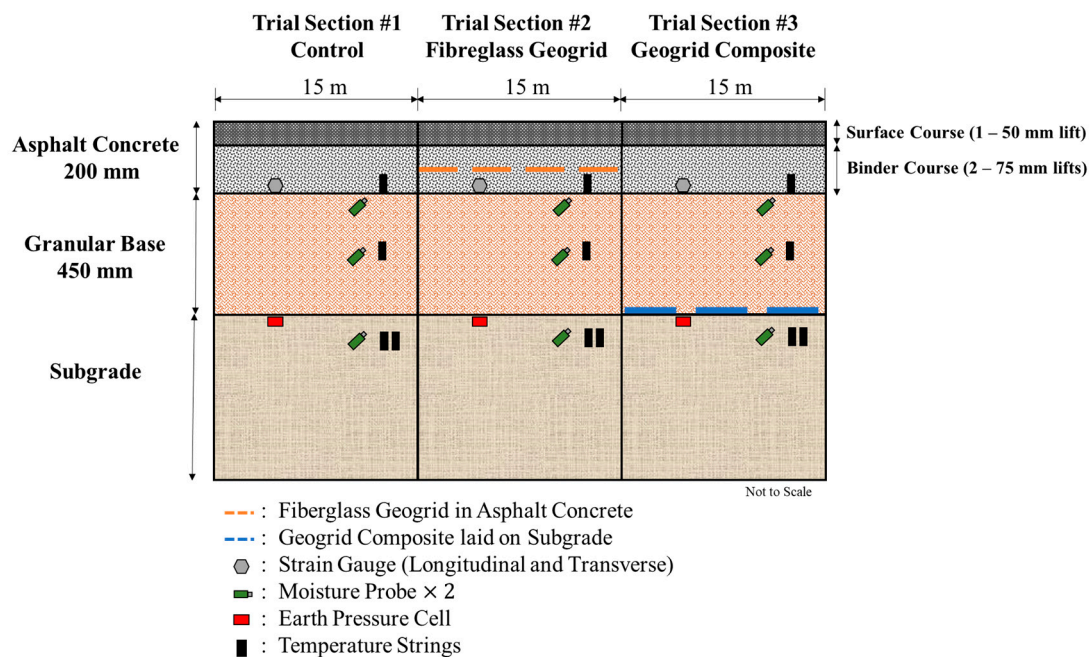


**Figure 1.** Section side view of field instrumentation and construction.

The use of fibreglass geogrid located at either the centre of the asphalt or geogrid composite on the subgrade can be an optimum solution for reconstructing a poor-condition pavement [30]. To better study this effect, three pavement structures were designed for the

trial sections in this project. These sections include a control section without reinforcement (referred to as Section 1, or the control section), a section with fibreglass geogrid installed within the two binder course lifts (referred to as Section 2, or the geogrid section), and the third section with geogrid composite laid at the interface of base and subgrade (referred to as Section 3, or the geogrid composite section). The fibreglass geogrid was installed in the asphalt layer to study its capability to reinforce asphalt concrete, while the geogrid composite bonded to geotextile has drainage and filtration functions, which is more crucial in the subgrade where water and fine particles can have a larger impact on the soil during freeze–thaw cycles.

Instrumentation was prepared to monitor the temperature, moisture, and mechanical behaviour of the pavement; instrumentation will be further detailed in Section 2.3. The cross-section side view showing detailed instrumentation profile and pavement structures is shown in Figure 1. All the sensors testing mechanical behaviour were installed along the right wheel path of the westbound lane. The data from the sensors were logged using a data logger installed in a cabinet located on the side of the roadway.

## 2.2. Geosynthetics Installation

Two types of geosynthetic materials were used in two test sections: a geogrid composite and a fibreglass geogrid. Section 3 was constructed first, and the geogrid composite was installed directly on the subgrade. The fibreglass geogrid was installed on Section 2 after paving the first binder course lift; it is located between the two lifts of SP 19 asphalt concrete.

### 2.2.1. Geogrid Composite on Subgrade

The geogrid composite was placed at the interface between the base and subgrade (Figure 2); from laboratory testing, the subgrade had a California Bearing Ratio (CBR) of 2%. The geogrid composite is made of biaxial polypropylene geogrid manufactured using a punching and drawing process, heat-bonded to a continuous filament non-woven polyester geotextile. The reinforcement is offered by the geogrid element while the mechanically and chemically stable geotextile acts as a filter/separator preventing the movement of fine soils in saturated soil [31].



**Figure 2.** Installation of geogrid composite on the subgrade.

As per the installation guide [32], the subgrade was prepared by removing debris, remnants, or any plants before installation. The surface was levelled and the geogrid composite was unrolled over the surface as shown in Figure 2. As each section is only 15 m, the manual installation of the geogrid composite material was challenging. As it is usually stored in rolls, the geogrid composite may not be completely flat when placed in the field and at least four workers were needed to hold each corner of the sheet during placement to reduce wrinkles. After rolling out the product, several shovels of fill were placed on the edges and corners to hold down the geogrid composite, as depicted in Figure 2. When necessary, adjacent geogrid composite rolls were overlapped by at least 500 mm [32].

It is not recommended for heavy equipment to directly drive on top of geogrid composite, especially when the subgrade is relatively soft. In this case, the granular

base material was first dumped and gradually pushed over the geogrid composite, with the dozer blade raising slowly to spread the fill material. After levelling the fill, more loads were dumped over the ground until it reached the design thickness as demonstrated in Figure 2. Finally, the base layer was compacted and graded to be ready for the asphalt placement. Using this construction procedure, it is recommended to sample granular materials after levelling the base surface and verify that no aggregate segregation occurs with gradation analysis. In addition, the lightweight deflectometer (LWD) testing was conducted; LWD results showed that the modulus for the base on top of the geogrid composite was consistent after installation.

### 2.2.2. Fibreglass Geogrid in Asphalt Binder Course (SP 19)

In this study, a biaxial fibreglass geogrid was used. This product is made of high-modulus glass filaments with a polymeric coating; the coated filaments are then bonded to an engineered polymeric membrane (EPM). The fibreglass geogrid has an opening of 25.4 mm × 25.4 mm, while the elastic modulus is 73,000 MPa and the ultimate tensile strength is 100 kN/m in both directions. During placement, the polymer-coated grids are placed directly on the asphalt surface after a tack coat is applied. As the EPM is designed to melt at elevated temperatures (around 80 °C), it provides more adhesion between the grids and asphalt overlays [33]. The product is stable mechanically, chemically, and biologically. This product is particularly engineered for asphalt reinforcement, where it can resist high temperatures with the polymer coating melting at temperatures >400 °C and the glass melting at 820 °C [33]

As shown in Figure 3, the first 75 mm lift of SP 19 was placed on the unreinforced graded base layer. A tack coat was placed on the first lift after one hour when the first lift had hardened and cooled down sufficiently. Due to the short length of this trial section, the tack coat was placed using hand rollers as shown in Figure 3 (left). The tack coat used in this study is Clean Bond Coat (CBC), which is a slow-setting asphalt emulsion and cures fast. It was diluted in a ratio of 50/50 with water. With the calculated one-lane pavement area of 50 m<sup>2</sup>, approximately 50 L of diluted tack coat was applied on one lane using hand rollers to ensure even application. This process was repeated twice until the lane was fully coated. After the tack coat was applied, it was allowed time to cure as indicated by a colour change from brown to black as depicted in Figure 3 (middle). For the proper installation of the fibreglass geogrid, it is important to not disturb the surface during curing; workers stepping and vehicles driving on tack-coated surfaces should be avoided. As such, the fibreglass geogrid was rolled out on the sidewalk first to minimize the potential loss of the tack coat during curing.

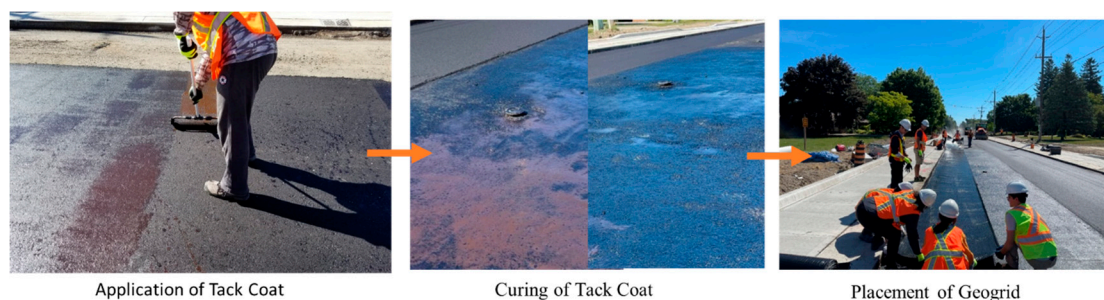


**Figure 3.** Installation of fibreglass geogrid in the asphalt.

After the tack coat was cured, the fibreglass geogrid was placed; several people held the edges of the geogrid to reduce wrinkles during placement as shown in Figure 3 [34]. Wrinkle removal is also critical to ensure the bonding between the geogrid and the underlying asphalt. Several measures were taken including a drum roller running on the entire length (Figure 4), a small hand roller rolling on the wrinkle (Figure 4), as well as cutting from the middle of the wrinkle. After the placement, the second binder course lift was paved.

The paver and other heavy equipment must be driven to the starting point of the paving direction before the tack coat application to prevent loss of the tack coat by the tires.



Drum Roller on the Geogrid

Hand Roller on the Wrinkle

Placing Loose Asphalt Mix on the Edges of Geogrids

**Figure 4.** Special measures taken during fibreglass geogrid installation.

Another challenge that occurred during the paving of the second lift overlying the geogrid was that, due to insufficient adhesion, the geogrid was lifted and picked up by the paver, which may be attributed to the tack coat not being fully cured before paving. Placing some loose asphalt mix in advance on the longitudinal and transverse edges of the geogrid, as shown in Figure 4, was found to improve the paving process. Using the same asphalt cement, as was used in the asphalt mixtures, as a tack coat could perform better than emulsions and provide better adhesion [33]. In the future, this method could be compared to the type of tack coat used in this study.

As per the manufacturer's recommendation, adjacent geogrids had at least 25 mm overlap. In this study, due to the width of the geogrid (i.e., 1.5 m), three sheets of the geogrid were needed on one lane, with two sheets at full width and one sheet of 0.9 m width. When placing the geogrid on the first lane, the geogrids were placed one after another, with the narrower one placed last, closest to the centreline. Due to the overlap of adjacent geogrids, some portions of the geogrid could not directly adhere to the tack-coated surface. As such, some parts of the narrower geogrid were picked up and lifted by the paver during the paving process for the first lane. During the installation of the geogrid in the second lane, the narrower geogrid was placed first in the middle of the lane with the other two sheets at full width placed on top, thus, the lifting issue was minimized. In this case, the narrower geogrid fully adhered to the tack coat. Future on-site non-destructive testing and visual inspection can be performed to compare the long-term performance of the two lanes.

### 2.3. Field Instrumentation

As shown previously in Figure 1, each section was instrumented to monitor the temperature, moisture, and mechanical behaviour during construction as well as the future life of the pavement. The following subsection details the installation of temperature strings, moisture probes, pressure cells and strain gauges in the trial sections.

#### 2.3.1. Temperature String

One temperature string was instrumented in the base lift of the binder course and the middle of the base layer. Two temperature strings were installed at 10 cm below the surface of the subgrade. In this case, 4 strings were installed in each section with a total of 12 strings installed in the three sections. The resistor of the calibrated temperature sensor was measured and converted to temperature based on the following equation:

$$T = \frac{1}{1.127355 \times 10^{-3} + 2.343978 \times 10^{-4} \ln R} + 8.674848 \times 10^{-8} \times (\ln R)^3 - 273.15, \quad (1)$$

where  $T$  represents the temperature ( $^{\circ}\text{C}$ );  $R$  represents the measured electrical resistance ( $\Omega$ ).

For the temperature sensors installed in the asphalt layer, heat shrink wrap was placed around the wire of the sensors as protection from the high paving temperatures. Before the pavement of the first lift, the sensor was buried in the top of the base layer with only a small portion exposed to protect it from heavy equipment when paving. The temperature sensors were dug out after the first lift was paved. Figure 5 illustrates one temperature sensor that was dug out. The sensors have an operating range from  $-55\text{ }^{\circ}\text{C}$  to  $+150\text{ }^{\circ}\text{C}$ .



**Figure 5.** Temperature sensor in the first lift of the binder course.

### 2.3.2. Moisture Probe

Two moisture probes were instrumented at three depths within the pavement structure: 10 cm below the surface of the subgrade, the middle of the base layer, and the top of the base layer. Therefore, 6 moisture probes were installed in each section and 18 moisture probes in total were instrumented in three sections. The probes used in this project are stable at temperatures below freezing. The moisture probes were programmed and calibrated in advance. The electrical resistance was measured and then the electrical resistance was calibrated to water potential as per Equation (2) [35].

$$\Psi = \begin{cases} 0, & \text{if } R < 0.55 \text{ k}\Omega \\ (R \times 23.156 - 12.736) \times [-1 - 0.018(T - 24)], & \text{if } 0.55 \text{ k}\Omega < R < 1 \text{ k}\Omega \\ \frac{-3.213 \times R - 4.093}{1 - 0.009733 \times R - 0.01205 \times T} & \text{if } 1 \text{ k}\Omega < R < 8 \text{ k}\Omega \\ -2.246 - 5.239 \times R \times (1 + 0.018 \times (T - 24)) - \\ 0.06756 \times R^2 \times [1 + 0.018 \times (T - 24)]^2, & \text{if } R > 8 \text{ k}\Omega \end{cases}, \quad (2)$$

where  $\Psi$  represents the water potential for the soil water tension in the pavement (kPa);  $R$  represents the measured electrical resistance (k $\Omega$ );  $T$  can be obtained from the measured temperature in the corresponding location by the temperature strings ( $^{\circ}\text{C}$ ). The calibrated moisture probes read water potential from 0 to 200 kPa, which represents the fluid flow potential, where a reading of 0 indicates the soil is saturated and 200 kPa indicates dry conditions.

Before installation, the probes were saturated in water for one hour and submerged in dry sand overnight, then they were saturated in the water again to activate the probes. Such a process was repeated several times until activation was successful. Finally, the moisture probes were conditioned by soaking in the water for at least 24 h before they were installed. To ensure saturation before the installation, the probes were soaked in plastic bags filled with water and fastened with zip ties allowing for transport to the site.

### 2.3.3. Total Earth Pressure Cell on Subgrade

One earth pressure cell was installed on the subgrade in each section, with three in total. The pressure cell can measure the stress on a plane surface; the installed pressure cells have an operating temperature range from  $-29\text{ }^{\circ}\text{C}$  to  $+65\text{ }^{\circ}\text{C}$ . The current can be measured

and converted to pressure by using the calibration equation provided by the manufacturer shown in Equation (3).

$$\sigma = mX + b, \quad (3)$$

where  $\sigma$  is the measured stress (MPa);  $X$  is the measured current (mA);  $m$  and  $b$  are calibration factors provided by the manufacturer, which stand for scale factor (MPa/mA) and offset (MPa), respectively. The calibrated readings show negative values when representing compressive stress.

The pressure cells were placed along the right wheel path (RWP). Fine sand was placed beneath the pressure cell to act as a flat base as well on the sensor to provide a stable environment for reading. Metal U-shaped pegs were used to hold the pressure cells in position, as shown in Figure 6. In Section 3, the geosynthetics were placed above the pressure cell to measure the benefit provided by the geogrid composite.

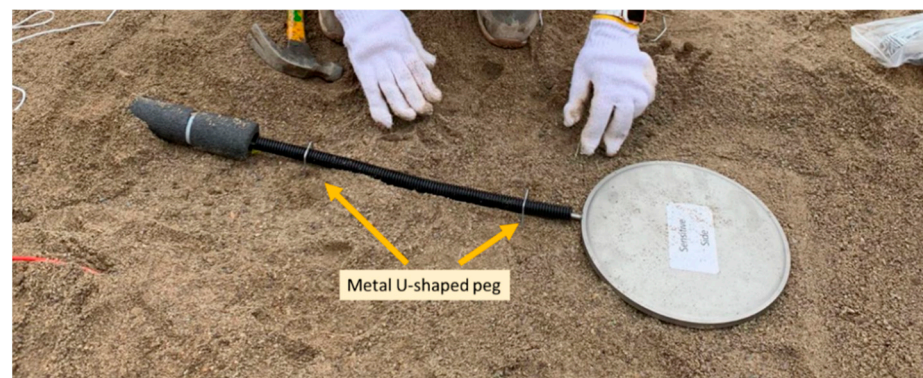


**Figure 6.** Installation of Pressure Cell.

#### 2.3.4. Dynamic Strain Gauges in Asphalt

Two strain gauges were installed in the base lift of the asphalt binder course, with one in the longitudinal and the other in the transverse direction. These strain gauges were designed to measure the horizontal axial strain under high-frequency loads and can work at temperatures ranging from  $-34\text{ }^{\circ}\text{C}$  to  $+200\text{ }^{\circ}\text{C}$ . High-temperature wires are used to ensure that the cabling will be undamaged from the high-temperature paving process. The strain gauges are all placed along the RWP.

These strain gauges were calibrated by zeroing the voltages first. The resultant voltage measured from the sensor was multiplied by the calibration factor (units:  $\mu\text{e}/\text{mV}/\text{V}$ ) provided by the manufacturer. A positive reading represents tensile strain, and a negative reading represents compressive strain. Like the installation of the temperature sensors in the asphalt, the strain gauges were dug out right after paving the first lift and before the asphalt cooled. Metal U-shaped pegs were used to hold the gauges in longitudinal and transverse directions. Care was taken to avoid vibration of the roller compactor directly on the sensors.

#### 2.3.5. Installation of Sensor Tree and Protection

To ensure that all the sensors measure the corresponding properties at the designed depth, a sensor “tree” was built for each section. The trees were made with PVC pipes with a diameter of 0.75 inches (19 mm). Branches were connected at specific heights of the tree with the sensors attached and all the wires can be accessed from the middle of the tree which is located at the top of the subgrade as illustrated in Figure 7. As seen in Figure 7, one temperature sensor and two strain gauges are located at the top of the tree that was buried in the asphalt. Two moisture probes are located at the branch at the top of the base layer. Two moisture probes and one temperature sensor are located at the branch in the middle of the base layer, which is approximately 22.5 cm from the top of the base layer. Then, one pressure cell is located at the top of the subgrade. Lastly, two moisture probes

and two temperature sensors are located at the branch that is 10 cm below the surface of the subgrade.

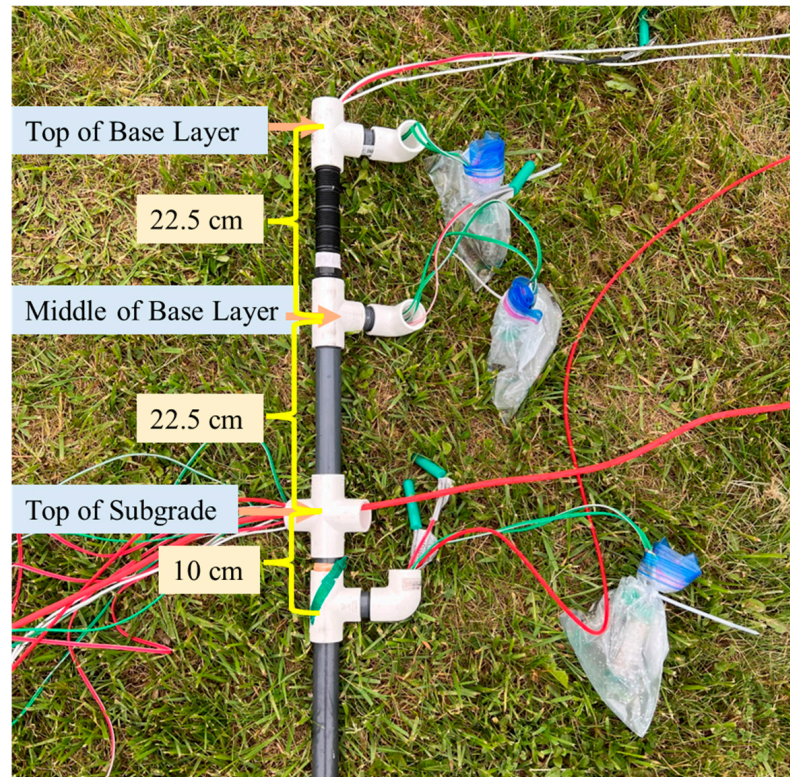


Figure 7. Sensor tree.

To install the sensor tree, a hole was dug from the subgrade and placed in the soil. The location of the tree was carefully examined to ensure the lowest branch of the tree was 10 cm below the surface of the subgrade. Then, the surrounding area of the tree was backfilled with excavated subgrade soil, as shown in Figure 8. The backfilled soil was manually compacted with a hand compactor. Wood boxes were used to cover the sensor trees temporarily to protect them from heavy equipment during construction. A similar procedure also was used to backfill and compact the granular base, as shown in Figure 8.

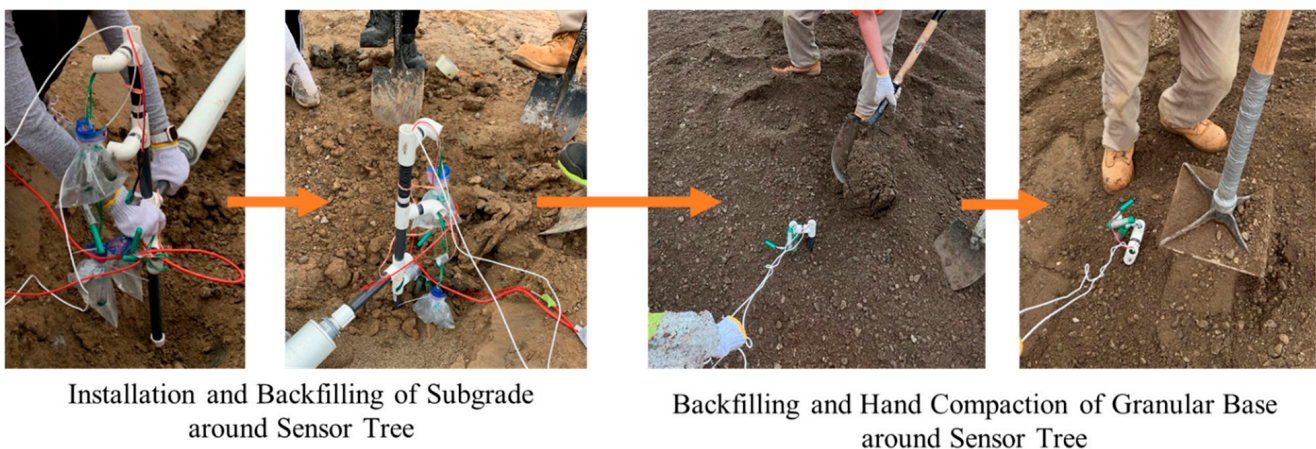
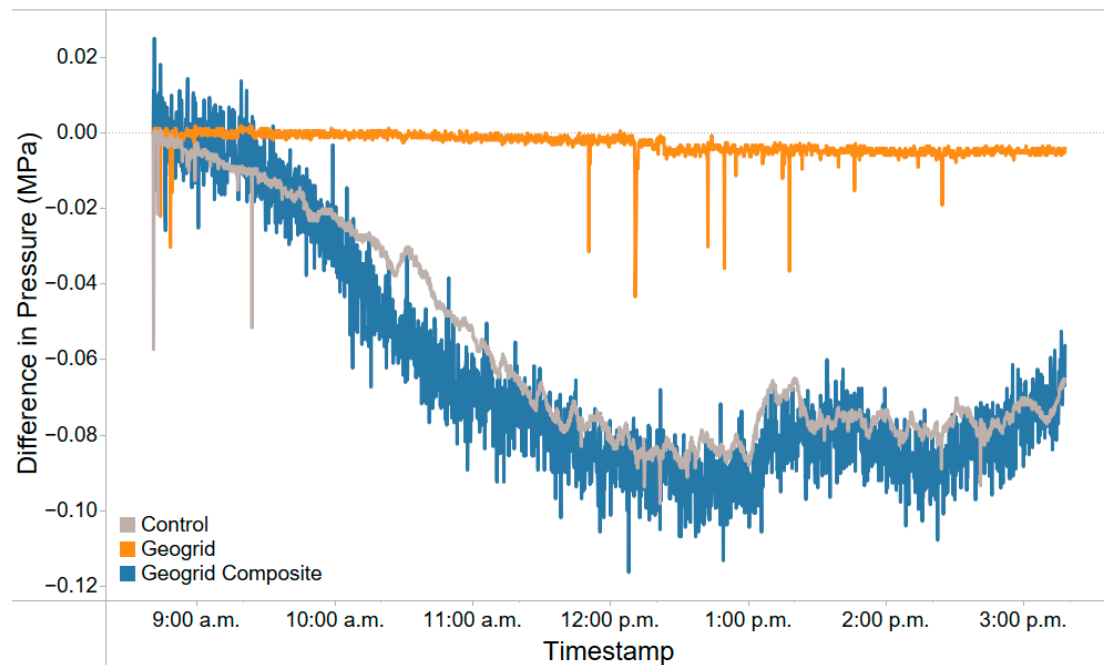


Figure 8. Installation of sensor tree.

### 3. Construction Impacts on the Geosynthetic–Reinforced Pavements

#### 3.1. Pressure at the Interface of Subgrade and Base

The readings of the pressure cells at the interface of the subgrade and base layer were taken during the construction of the asphalt binder course (SP 19), and asphalt surface layer (SP 12.5). The data were collected every 10 s during the construction of the binder course and every minute during the construction of the surface layer. Although the traffic volume and construction truck specifications were not available, the construction equipment was consistent for all sections during each stage of construction by designating equipment to a specific lane in the test sections. All other construction traffic was kept on the lane that was not instrumented during the data collection period. By taking the difference between an individual sensor reading at the time,  $t$ , and the first reading before construction, the readings of the pressure cells during construction of the asphalt binder course were plotted in Figure 9. Figure 9 details the readings from approximately 8:30 a.m. until 3:30 p.m. corresponding to the start and finish of construction, respectively.



**Figure 9.** Pressure at the Interface of Subgrade and Base during Binder Course Construction.

The construction timeline can be observed more clearly from the pressure readings of control and geogrid composite sections. The pressure increase ending at approximately 1 p.m. corresponds to the paving and compaction of asphalt concrete. During this time, the contribution of the geogrid composites on the subgrade as well as the fibreglass geogrid in the binder course can be inferred. It can be observed that the geogrid composite section (Section 3) shows more noise but with a similar trend to the control section, and experiences a maximum pressure of approximately 0.10 MPa. However, the pressure cell on the subgrade in the fibreglass geogrid section (Section 2) experienced a much lower pressure (0.03 MPa). Due to the absence of the paver and compaction equipment, the pressure levelled out as shown in the control and geogrid composite sections. During the paving of the binder course, the geogrid section experienced approximately 70% lower pressure on the subgrade compared with the other two sections, which may be attributed to the fibreglass geogrid reducing the impact of heavy construction trucks on the base and subgrade. It is believed that these measurements demonstrate the ability of the fibreglass geogrid to distribute the load and provide reinforcement during construction.

Figure 10 shows the readings of the pressure cells collected during the construction of the asphalt surface course. From these results, a similar level of noise was demonstrated in all three sections. This may be attributed to the different data collection frequency (i.e., one measurement per minute) from the previous two construction activities. As shown in Figure 10, the trends of all three pressure cells are similar; however, larger peak pressure values were observed in the control section and geogrid composite sections.

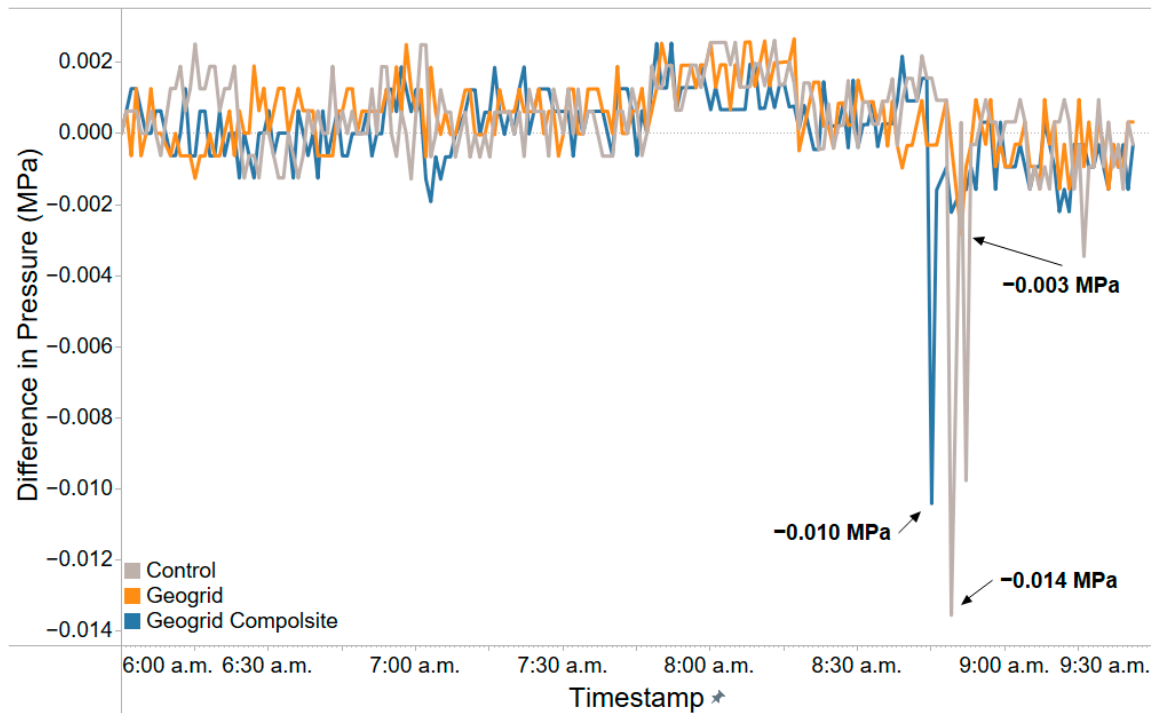


**Figure 10.** Pressure at the interface of subgrade and base during surface course construction.

### 3.2. Strain within the Asphalt Binder Course

The readings of the strain gauges (longitudinal and transverse) installed in the binder course were taken during the construction of the asphalt binder course (SP 19), and asphalt surface layer (SP 12.5). The data were collected every 10 s during the construction of the binder course, and it was collected every minute during the construction of the surface layer. Similar to the process of data of pressure cells, the measurements were offset to the zero point using the first reading. A positive result indicates the tensile strain, while a negative value indicates the compressive strain. The readings of the asphalt strain gauges during the construction of the binder course are plotted in Figure 11. These results reflect the impacts of the fibreglass geogrid in the binder course when stress was exerted on them. The readings taken from both longitudinal and transverse gauges illustrate similar trends in the three sections. The gauges were experiencing compressive strains from 9 a.m. to around 12:30 p.m., which matches the construction timeframe discussed previously in regard to Figure 9.

Due to the completion of construction activities as well as the viscoelastic nature of asphalt materials, the strains experienced at the bottom of the asphalt layer increase after 1 p.m. In the transverse direction, the fibreglass geogrid section (Section 2) experienced lower strains during the construction. It is also notable that some exceptionally high values were exhibited in the control section in the longitudinal direction. This observation aligns with previous studies that demonstrated that the longitudinal strain is typically higher than the transverse values [36,37].

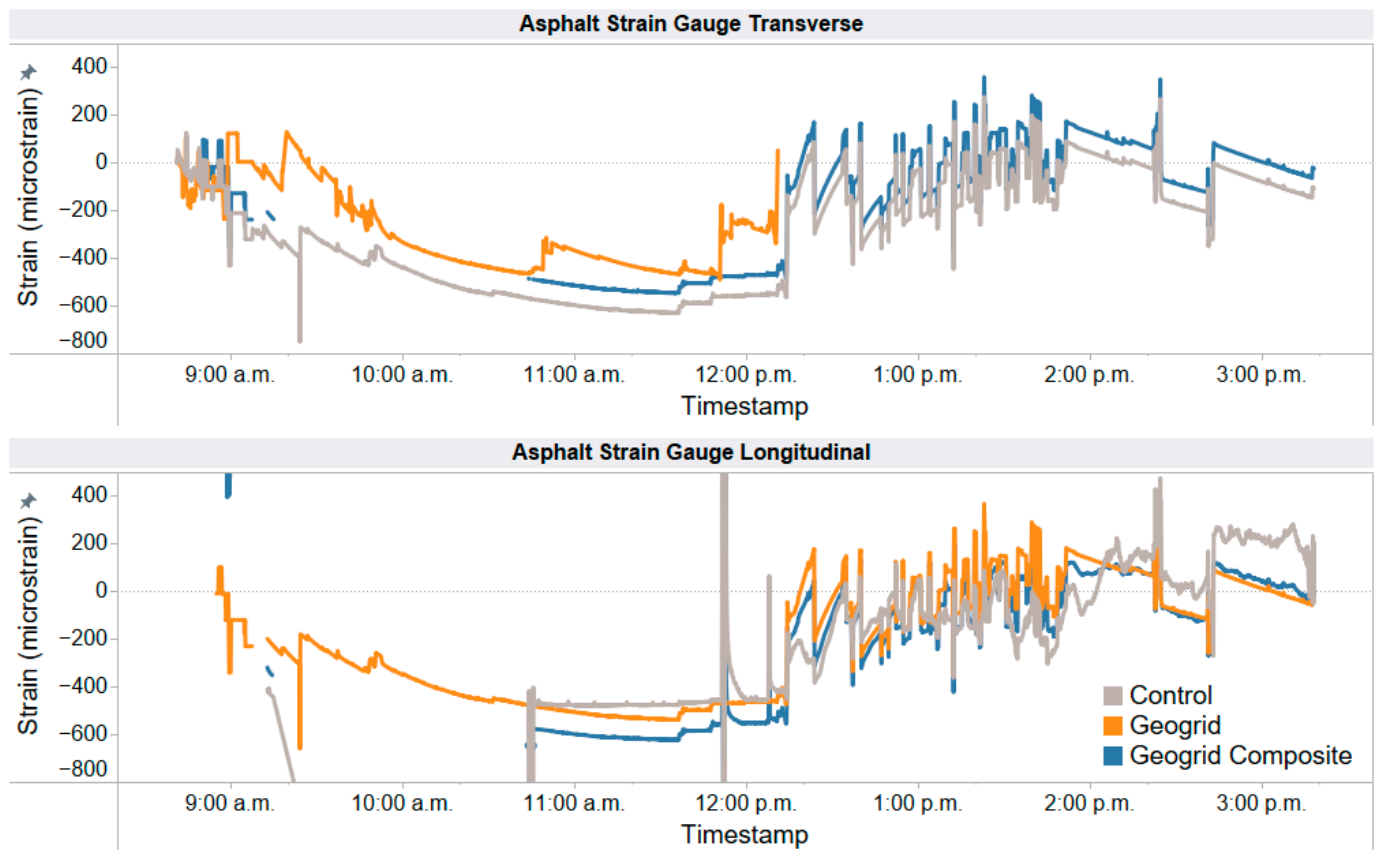


**Figure 11.** Asphalt strain gauge reading during binder course construction.

Figure 12 shows the readings of the asphalt strain gauges collected during the construction of the surface course. Similar to the reading of pressure cells, lower noise was observed due to a lower frequency of data collection, although this could also be attributed to the additional thickness of surface course material being paved. In the transverse direction, the control and geogrid composite sections both measure high strain values around 7:10 a.m. Other than these peak values, the tensile strain experienced at the bottom of the binder course reached the highest level during paving after 8:00 a.m., with the fibreglass geogrid section showing a lower level of strain. A similar trend is also exhibited in the longitudinal direction.

As shown in Figure 12 (top), the transverse strain in the binder course caused by the construction of the surface course is reduced in the fibreglass geogrid section by more than 99% compared with the other two sections. As the fibreglass geogrid-reinforced asphalt course can better distribute stresses under loading, this leads to less disturbance to the binder course, granular base, and subgrade. In the longitudinal direction, the fibreglass geogrid can reduce about 54% and 50% strain compared with control and geogrid composite sections.

Although higher strains in longitudinal directions are typically observed, higher longitudinal strains may also be attributed to the aperture size spacing of the longitudinal filaments of the geogrids; larger apertures may reduce the interaction between grid filaments improving the pull-out resistance in the longitudinal direction. However, the spacing between transverse members has little impact on the pull-out resistance [38,39]. With regards to the lower strain level experienced in both longitudinal and transverse directions, the results align with the pressure cell measurements observed in Figure 10, which signifies the impacts of load distribution provided by the fibreglass geogrid on the RWP.

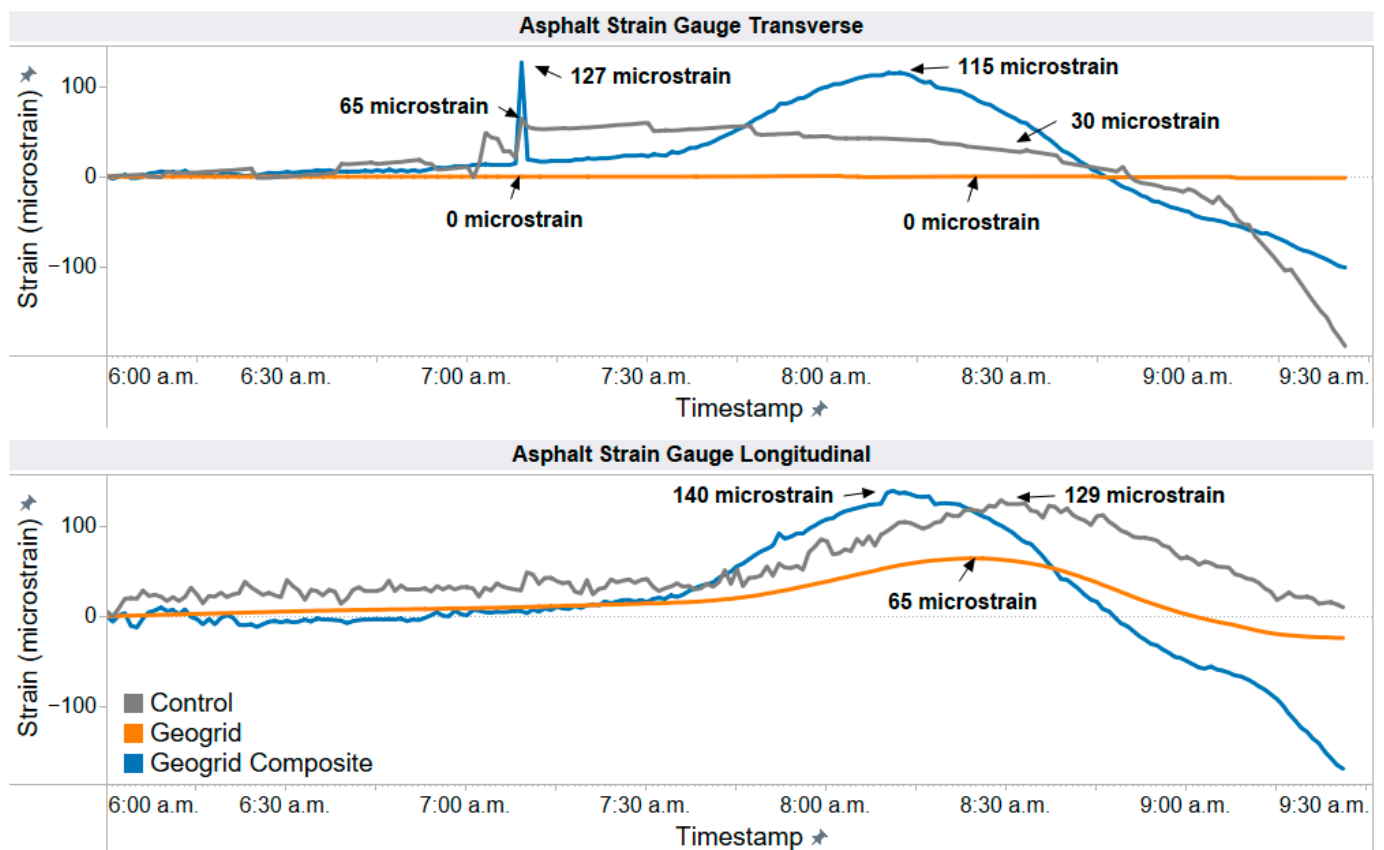


**Figure 12.** Asphalt strain gauge reading during surface course construction.

### 3.3. Moisture

The readings of the moisture probes installed at the top of the granular base layer, middle of the granular base layer, and 10 cm below the subgrade were taken during the construction of the asphalt surface layer (SP 12.5). Data were collected every minute during construction. Lower moisture values represent a more saturated probe, which can provide information about the drainage capability of both fibreglass geogrid and geogrid composites.

The water potential profile in the pavement structure based on each section and each layer is plotted in Figures 13 and 14. The measured water potential in the subgrade in all three sections is close to 0 (i.e., almost fully saturated) while the drainage behaviour can be observed in the geogrid composite section (Section 3). It can also be observed that the water potential in the subgrade in the geogrid composite is slightly higher, indicating a drier condition. At the middle of the base layer, the geogrid composite section generally shows a drier condition, with the control section showing a saturated condition. Lastly, at the top of the base layer, the geogrid composite is very much drier. The water potential readings in the fibreglass geogrid and control sections are close, with a slightly higher water potential in the fibreglass geogrid section. As the geogrid composite material serves as both a filter and separator, the water drains downwards more quickly, but it also prevents the upward migration of moisture and fine soils. As the same granular and asphalt material was used in all sections, the improved drainage behaviour can be attributed to the geogrid composite material installed in Section 3, thus, demonstrating the potential of the geogrid composite to mitigate the consequences of freeze–thaw cycles in the future. This observation can be confirmed when monitoring the water potential of the geogrid composite section during the colder winter months after construction.

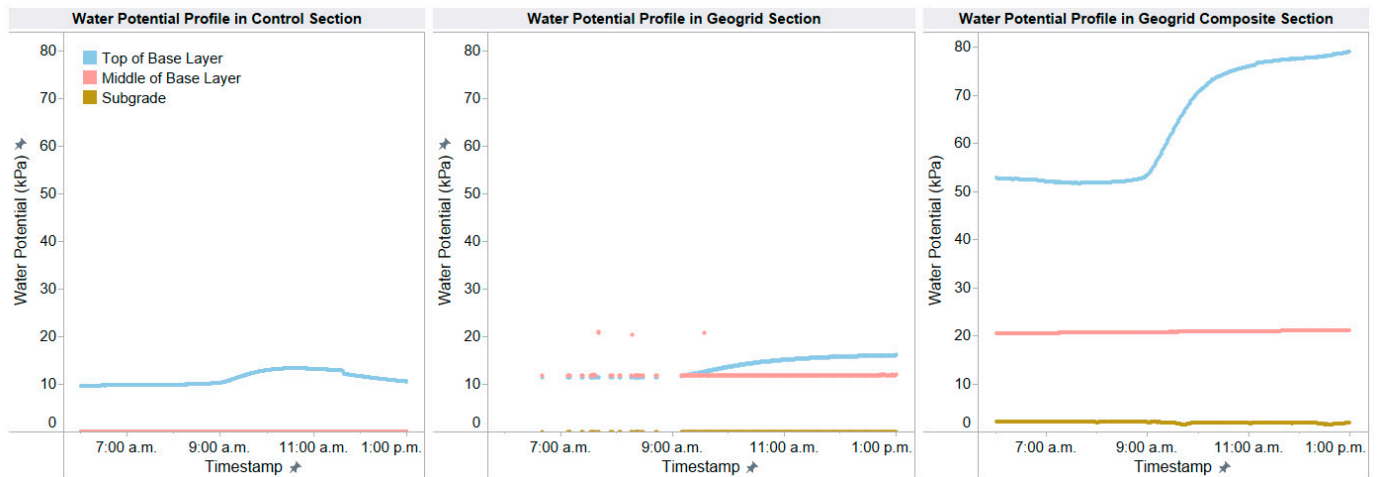


Figure 13. Water potential profile for each section during surface course construction.

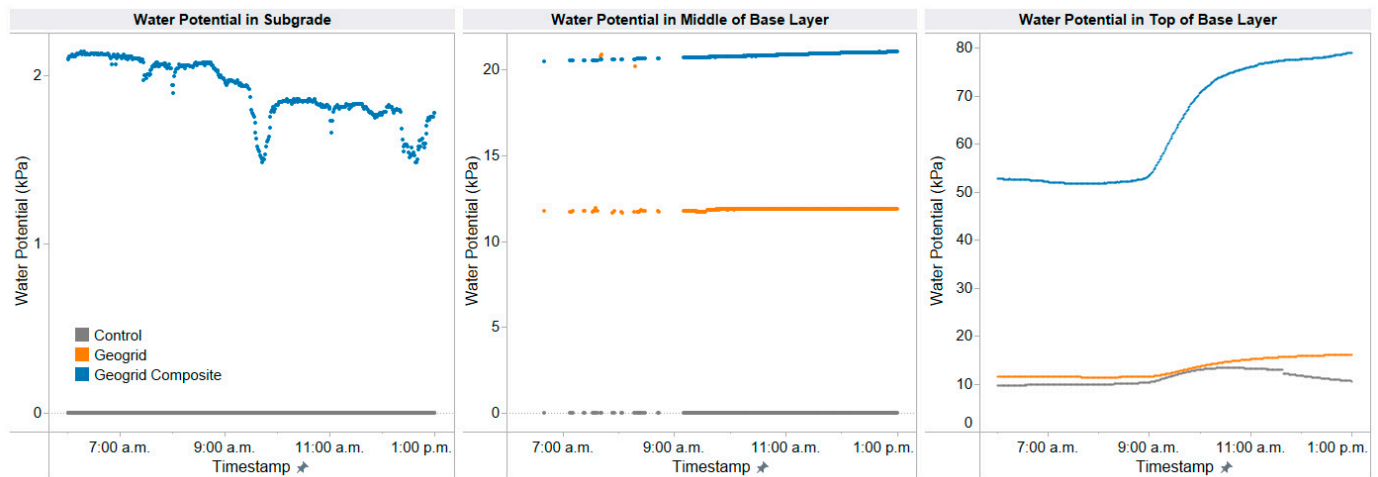


Figure 14. Water potential in each layer during surface course construction.

### 3.4. Temperature

The readings of the temperature sensors installed in the base lift of the binder course, the middle of the granular base layer, and 10 cm below the subgrade were taken every minute during the construction of the asphalt surface layer (SP 12.5).

The temperature in different sections was plotted based on each layer in Figure 15. It can be observed that the temperature in the subgrade in the geogrid composite is the lowest. These results may indicate the indirect insulation potential of these materials provided by the drainage effect. As discussed previously, the moisture conditions in these sections shown in Figure 13 also contribute to the temperature change in the three sections. From the results, the geogrid composite exhibits a lower temperature in the subgrade and middle of the base layer which may be attributed to the filtering, draining, and inhibiting upward migration of moisture and fine particles. This is especially beneficial for the climate conditions in Canada, which can lead to freeze and thaw cycles in the pavement during winter. However, as the data were collected during construction, which was a relatively short period, long-term monitoring is necessary to evaluate the freeze-thaw impacts on geosynthetic-reinforced pavements and to verify this observation.

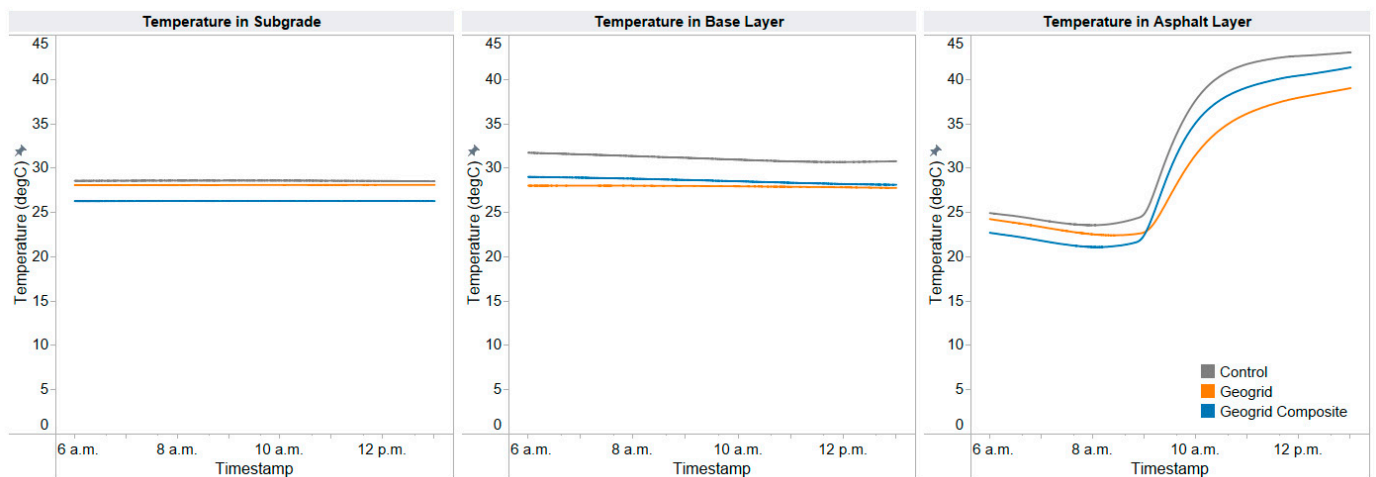


Figure 15. Temperature in each layer during surface course construction.

#### 4. Post-Construction Impact Assessment

##### 4.1. Light Weight Deflectometer Testing

A Light Weight Deflectometer (LWD) can be used to measure the stiffness of the subgrade, base, and pavement by releasing and applying loads on the pavement surface. Deflections are measured when a 20 kg weight is dropped from a height of 100 cm. The sudden drop of the weight transmits a stress pulse to the ground, and the deflection can be used to calculate the modulus at the surface. A 300 mm diameter plate was used when performing the testing on the subgrade and granular base. A 200 mm diameter plate was used for the testing on the binder course and surface course. The tests were performed on both the left wheel path (LWP) and the right wheel path (RWP) on the westbound lane. Fewer points were tested on subgrade and base due to the consistent outcomes, while the LWD was performed every 5 m along the lane on both wheel paths on the binder course and surface course. At least three measurements were taken from one location before moving to a new location. Prior to the installation, the stiffness values were shown in Figure 16. The control section had the stiffest subgrade and the geogrid composite section showed the weakest subgrade. The weaker subgrade in the geogrid composite section (Section 3) is consistent with the higher level of pressure experienced on the subgrade (Figure 9) and higher horizontal tensile strain experienced at the bottom of the binder course (Figure 12).

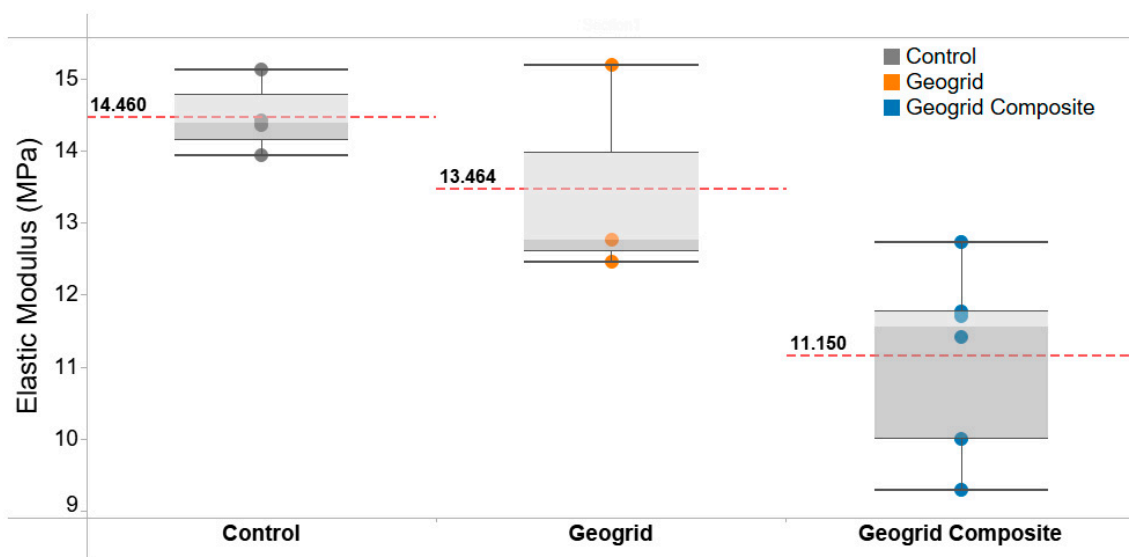


Figure 16. LWD results tested on compacted subgrade.

The deduced surface moduli after the placement of the asphalt surface course are plotted in Figure 17. From these measurements, the geogrid composite section shows the lowest stiffness measurements which is consistent with weak subgrade measurements as indicated in Figure 16. It can be observed that the fibreglass geogrid section (Section 2) exhibits the highest measurements in surface moduli further indicating the benefit of the fibreglass geogrid within the asphalt layer and its ability to mitigate of the impact construction activities.

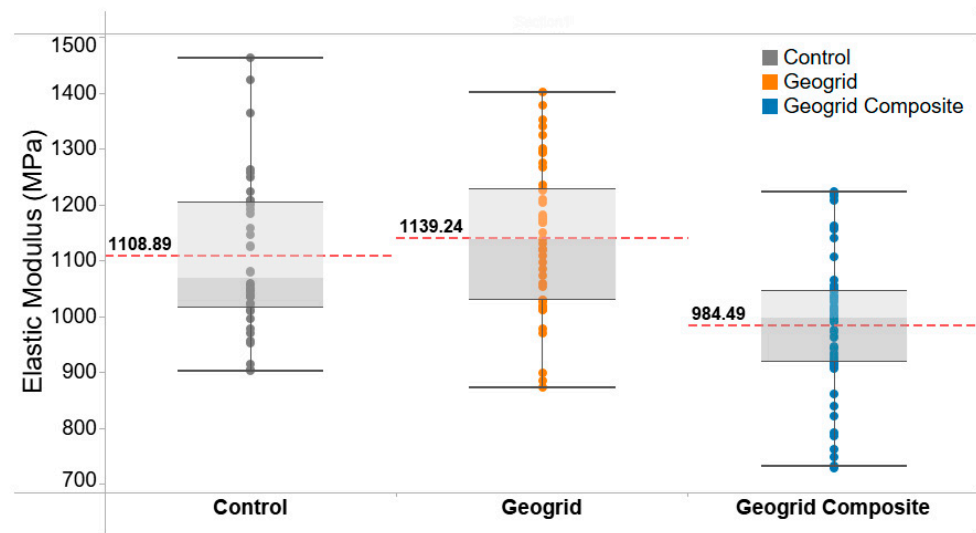


Figure 17. LWD results tested after surface course construction.

#### 4.2. Instrumentation Monitoring

To verify the functionality instrumentation installed during construction and the reliability of the data present in the previous section, data collected from each sensor two weeks after the last construction activity (i.e., paving of asphalt surface course) are shown in Figure 18. The frequency of data logging after construction was 5 min. The mechanical sensors were analysed by taking the difference from the previous reading to show the changes in pressure or strains.

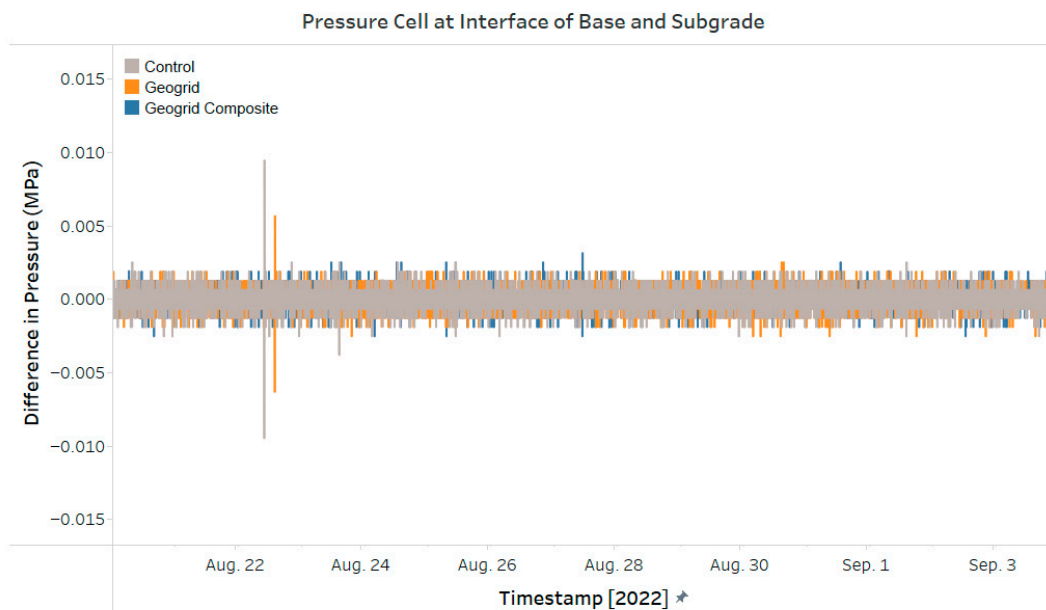


Figure 18. Cont.

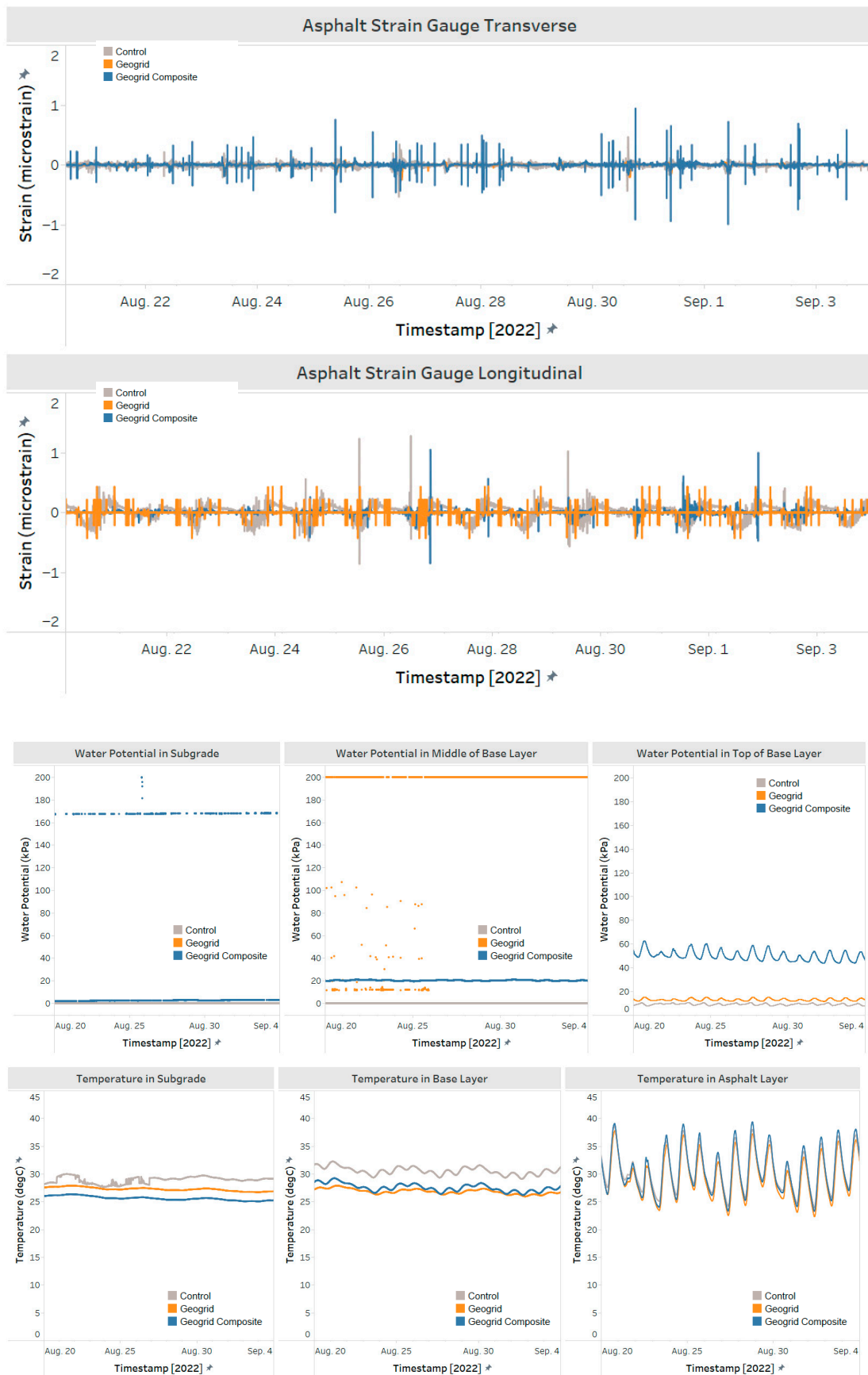


Figure 18. Instrumentation readings post-construction.

From the figure, the pressure cell shows stable readings during two weeks after construction. Two pressure spikes were observed in the control section and another one in the fibreglass geogrid section; however, it is unclear as to the cause of these spikes. Long-term monitoring will be more beneficial to capture more pressure changes in each section and to reduce the prevalence of these spikes. The asphalt strain gauges show higher transverse strain in the geogrid composite section and higher longitudinal strain in both the control and geogrid composite sections. To visualize the mechanical response more clearly, data can be collected at a higher frequency to capture a single and identical loading in all three sections.

From the readings of environment sensors (moisture probes and temperature strings), the subgrade in the control and fibreglass geogrid section was fully saturated, with a marginally drier subgrade in the geogrid composite section. The temperature in the asphalt layer in the three sections is similar, while that in the control section in the base layer and subgrade is higher than the other two sections. This can be attributed to the saturated condition in the base and subgrade in the control section.

## 5. Conclusions

In general, this paper develops the procedures and techniques to perform a full-scale field study regarding the geosynthetics-reinforced pavement in Southern Ontario, Canada. This paper describes the installation practices of the geogrid composite installed on the subgrade and a fibreglass geogrid installed in the asphalt binder course. More measures and caution should be taken during the installation of fibreglass geogrid within the asphalt to ensure the bonding of the fibreglass geogrid with the asphalt. This full-scale study also introduces instrumentations for long-term monitoring in Canada. The calibration and installation of the sensors were presented, including temperature strings, moisture probes, pressure cells, and asphalt strain gauges.

The results collected during construction were analysed and some field tests were performed to show the impacts of geosynthetics, as listed below:

- The readings taken from pressure cells on the subgrade show that the fibreglass geogrid in the binder course can diminish the mechanical disturbances vertically from the construction of the binder course and surface course by distributing the load. The geogrid composite can offer little reinforcement of the entire structure during the construction with a similar pressure reading as observed in the control section.
- The horizontal strain in the first lift of the binder course caused by construction activities of asphalt placement can be significantly reduced by the fibreglass geogrid installed between the two lifts of the binder course in the transverse direction, with some reduction in the longitudinal direction. The geogrid composite section shows similar horizontal strain values in the binder course during construction with the control section.
- Geogrid composite on the subgrade shows improved drainage capability and produces a distinct water potential profile within the pavement structure. The drainage, filtration, and inhibition of upward migration of moisture and fine particles were observed in the geogrid composite section with drier conditions in different depths of the pavements. This indicates an improved performance of the pavements undergoing freeze–thaw cycles and can be verified with future fieldwork at the site.
- From the temperature monitoring, the geogrid composite shows indirect insulation capability due to the drainage effect provided by the geotextile, which may decrease the potential for severe freeze–thaw damage. This observation will have to be verified using the long-term monitoring of the pavement sections.
- The results of LWD testing indicate the reinforcement of the fibreglass geogrid with the highest stiffness measurements after the asphalt placement. Future fieldwork can be used to determine the long-term benefits of the geosynthetic.
- Data collected during two weeks after construction verified that all instrumentations were functioning as expected. A longer monitoring process would be beneficial to eval-

uate the pavement performance to reduce the prevalence of outliers and spikes in the sensor measurements. Furthermore, further field investigations are recommended to study the long-term behaviour of geosynthetic-reinforced pavements. Non-destructive pavement evaluation techniques can be used to evaluate the permanent deformation under the traffic loading, and the fatigue damage caused by the repetitive loading. Based on the moisture and temperature results, long-term monitoring will also be beneficial to evaluate the performance of the pavement sections after they experience freeze–thaw cycles to investigate the ability of geosynthetic composites to mitigate freeze–thaw.

- With certain financial and technical constraints, which limited the ability to employ a larger number of sensors to provide duplication, it is recommended to verify the mechanical responses obtained from the strain gauges and pressure cells by applying certain traffic loading on the pavements; it can also help monitor the performance of in-service pavements.

**Author Contributions:** Conceptualization, D.W.; methodology, D.W. and S.-L.W.; formal analysis, D.W.; data curation, D.W.; resources, S.B.; writing—original draft preparation, D.W.; writing—review and editing, D.W., S.-L.W., S.B., S.T. and S.Y.; supervision, S.T. and S.Y.; project administration, S.T. and S.Y.; funding acquisition, S.T. and S.Y. All authors have read and agreed to the published version of the manuscript.

**Funding:** The research is supported by a Natural Sciences and Engineering Research Council of Canada (NSERC) Alliance Grant co-funded by Titan Environmental Ltd. The authors are also grateful to Titan Environmental Containment Ltd., for supplying the geogrid material and providing technical support for this project.

**Institutional Review Board Statement:** Not applicable.

**Informed Consent Statement:** Not applicable.

**Data Availability Statement:** Not applicable.

**Conflicts of Interest:** Titan Environmental Ltd. (Sam Bhat) has provided the customized products and provided the overall technical guidance using the geosynthetics for the project. The remaining authors declare no conflict of interest.

## References

1. Ghafoori, N.; Sharbaf, M. *Use of Geogrid for Strengthening and Reducing the Roadway Structural Sections*; Department of Transportation: Carson City, NV, USA, 2016.
2. Behera, B.; Nanda, R.P. Geogrid Reinforced Brick Buildings for Earthquake Disaster Mitigations. *Case Stud. Constr. Mater.* **2022**, *16*, e01113. [[CrossRef](#)]
3. Han, J.; Akins, K. Use of Geogrid-Reinforced and Pile-Supported Earth Structures. In *Deep Foundations 2002: An International Perspective on Theory, Design, Construction, and Performance*; ASCE: Reston, VA, USA, 2002; pp. 668–679. [[CrossRef](#)]
4. Jain, S.K.; Nusari, M.S.; Shrestha, R.; Mandal, A.K. Use of RCC Pile, Anchor Bolt and Geogrid for Building Construction on the Unstable Slope. *Geoenviro. Disasters* **2023**, *10*, 13. [[CrossRef](#)]
5. Das, B.M. Use of Geogrid in the Construction of Railroads. *Innov. Infrastruct. Solut.* **2016**, *1*, 1–12. [[CrossRef](#)]
6. Caltabiano, M.A.; Brunton, J.M. *Reflection Cracking in Asphalt Overlays*; Association of Asphalt Paving Technologists Technical Sessions: Seattle, WA, USA, 1991; Volume 60.
7. Brown, S.F.; Thom, N.H.; Sanders, P.J. *A Study of Grid Reinforced Asphalt to Combat Reflection Cracking*; Association of Asphalt Paving Technologists Technical Sessions: Seattle, WA, USA, 2001; Volume 70, pp. 543–571.
8. Sobhan, K.; Tandon, V. Mitigating Reflection Cracking in Asphalt Overlays Using Geosynthetic Reinforcements. *Road Mater. Pavement Des.* **2008**, *9*, 367–387. [[CrossRef](#)]
9. Lee, S.J. Mechanical Performance and Crack Retardation Study of a Fiberglass-Grid-Reinforced Asphalt Concrete System. *Can. J. Civ. Eng.* **2008**, *35*, 1042–1049. [[CrossRef](#)]
10. Arsenie, I.M.; Chazallon, C.; Duchez, J.L.; Mouhoubi, S. Modelling of the Fatigue Damage of a Geogrid-Reinforced Asphalt Concrete. *Road Mater. Pavement Des.* **2016**, *18*, 250–262. [[CrossRef](#)]
11. Darzins, T.; Qiu, H.; Xue, J. A Preliminary Laboratory Study of Fatigue Performance of Geogrid-Reinforced Asphalt Beam. In *Proceedings of the 6th GeoChina International Conference on Civil & Transportation Infrastructures: From Engineering to Smart & Green Life Cycle Solutions*, Nanchang, China, 19–21 July 2021; pp. 67–77. [[CrossRef](#)]

12. Kumar, V.V.; Saride, S.; Zornberg, J.G. Fatigue Performance of Geosynthetic-Reinforced Asphalt Layers. *Geosynth. Int.* **2021**, *28*, 584–597. [CrossRef]
13. Li, Q.; He, Y.; Yang, G.; Su, P.; Li, B. The Cracking Resistance Behavior of Geosynthetics-Reinforced Asphalt Concrete under Lower Temperatures Using Bending Test. *Coatings* **2022**, *12*, 812. [CrossRef]
14. Jayalath, C.; Gallage, C.; Wimalasena, K.; Lee, J.; Ramanujam, J. Performance of Composite Geogrid Reinforced Unpaved Pavements under Cyclic Loading. *Constr. Build. Mater.* **2021**, *304*, 124570. [CrossRef]
15. Jayalath, C.P.G.; Gallage, C.; Wimalasena, K. Development of Design Guidelines for Composite-Geogrid Reinforced Unpaved Pavements. In *Road and Airfield Pavement Technology*; Springer: Berlin/Heidelberg, Germany, 2022; Volume 193, pp. 375–387. [CrossRef]
16. Perkins, S.W.; Perkins, S.W. *Geosynthetic Reinforced Flexible Pavement Systems Using Two Pavement Test Facilities*; Federal Highway Administration: Bozeman, MT, USA, 2002.
17. Aran, S. Geosynthetics: Soil and Aggregate Reinforcement Testing—Base Reinforcement with Biaxial Geogrid. *Transp. Res. Rec. J. Transp. Res. Board.* **2006**, *1975*, 115–123. [CrossRef]
18. Al-Qadi, I.L.; Dessouky, S.H.; Kwon, J.; Tutumluer, E. Geogrid in Flexible Pavements: Validated Mechanism. *Transp. Res. Rec.* **2008**, *2045*, 102–109. [CrossRef]
19. Al-Qadi, I.L.; Dessouky, S.H.; Kwon, J.; Tutumluer, E. Geogrid-Reinforced Low-Volume Flexible Pavements: Pavement Response and Geogrid Optimal Location. *J. Transp. Eng.* **2012**, *138*, 1083–1090. [CrossRef]
20. Alimohammadi, H.; Schaefer, V.R.; Zheng, J.; Li, H. Performance Evaluation of Geosynthetic Reinforced Flexible Pavement: A Review of Full-Scale Field Studies. *Int. J. Pavement Res. Technol.* **2021**, *14*, 30–42. [CrossRef]
21. Correia, N.S.; Zornberg, J.G. Mechanical Response of Flexible Pavements Enhanced with Geogrid-Reinforced Asphalt Overlays. *Geosynth. Int.* **2016**, *23*, 183–193. [CrossRef]
22. Lai, Y.; Zhang, S.; Yu, W. A New Structure to Control Frost Boiling and Frost Heave of Embankments in Cold Regions. *Cold Reg. Sci. Technol.* **2012**, *79–80*, 53–66. [CrossRef]
23. Tingle, J.S.; Webster, S.L. Corps of Engineers Design of Geosynthetic-Reinforced Unpaved Roads. *Transp. Res. Rec.* **2003**, *1849*, 193–201. [CrossRef]
24. Pasquini, E.; Pasetto, M.; Canestrari, F. Geocomposites against Reflective Cracking in Asphalt Pavements: Laboratory Simulation of a Field Application. *Road Mater. Pavement Des.* **2015**, *16*, 815–835. [CrossRef]
25. Lakkavalli, V.; Bhat, S.; Thomas, J. The City of Calgary’s Early Experiences with Use of Fiberglass Grids for Asphalt Pavement Rehabilitation. In Proceedings of the Geosynthetics 2018—2nd International Conference on Technology and Application of Geosynthetics, Santiago, Chile, 3–5 October 2018.
26. Gonzalez-Torre, I.; Calzada-Perez, M.A.; Vega-Zamanillo, A.; Castro-Fresno, D. Damage Evaluation during Installation of Geosynthetics Used in Asphalt Pavements. *Geosynth. Int.* **2015**, *21*, 377–386. [CrossRef]
27. OPSS, OPSS 1151; Material Specification for Superpave and Stone Mastic Asphalt Mixtures. Ontario Provincial Standard Specifications (OPSS): Ottawa, ON, Canada, 2006.
28. OPSS, OPSS 1010; Material Specification for Aggregates-Base, Subbase, Select Subgrade, and Backfill Material. Ontario Provincial Standard Specifications (OPSS): Ottawa, ON, Canada, 2013.
29. Pinchin Ltd. *Geotechnical Investigation-Proposed Snyder’s Road Reconstruction*; Pinchin Ltd.: Edmonton, AB, USA, 2020.
30. Bhat, S.; Thomas, J. Design and Construction of a Geosynthetic Reinforced Pavement on Weak Subgrade. In Proceedings of the Canadian Geotechnical Conference & Canadian Permafrost Conference, Quebec City, QC, Canada, 20–23 September 2015.
31. Titan Environmental Containment. Swamp Grid 30. 2021. Available online: [https://www.google.com.hk/url?sa=t&rct=j&q=&esrc=s&source=web&cd=&cad=rja&uact=8&ved=2ahUKewiyI7CT0KmBAXU4qFYBHfYbDg8QFnoECBgQAQ&url=https%3A%2F%2Ftitanenviro.com%2Fwp-content%2Fuploads%2F2021%2F07%2FSwamp-Grid-30\\_February2021.pdf&usg=AOvVaw1zuExkHYMnQ6SregPuO-N9&opi=89978449](https://www.google.com.hk/url?sa=t&rct=j&q=&esrc=s&source=web&cd=&cad=rja&uact=8&ved=2ahUKewiyI7CT0KmBAXU4qFYBHfYbDg8QFnoECBgQAQ&url=https%3A%2F%2Ftitanenviro.com%2Fwp-content%2Fuploads%2F2021%2F07%2FSwamp-Grid-30_February2021.pdf&usg=AOvVaw1zuExkHYMnQ6SregPuO-N9&opi=89978449) (accessed on 21 March 2023).
32. Titan Environmental Containment. Installation Guide for Base Reinforcement. 2022. Available online: [https://titanenviro.com/wp-content/uploads/2022/03/Titan-Earth-Grid-Swamp-Grid-and-Gladiator-Grid-Installation-Guide\\_Base-Reinforcement\\_22Feb2022.pdf](https://titanenviro.com/wp-content/uploads/2022/03/Titan-Earth-Grid-Swamp-Grid-and-Gladiator-Grid-Installation-Guide_Base-Reinforcement_22Feb2022.pdf) (accessed on 21 March 2023).
33. Titan Environmental Containment. Spartan Road GridTM 11EPM. 2017. Available online: [https://www.google.com.hk/url?sa=t&rct=j&q=&esrc=s&source=web&cd=&cad=rja&uact=8&ved=2ahUKewj8xMfA0KmBAXVSr1YBHWIABHAQFnoECB4QAQ&url=https%3A%2F%2Ftitanenviro.com%2Fwp-content%2Fuploads%2F2021%2F05%2FSpartan-Road-Grid-11EPM\\_March2021.pdf&usg=AOvVaw00i\\_jFhXVeYb0w6JBme79H&opi=89978449](https://www.google.com.hk/url?sa=t&rct=j&q=&esrc=s&source=web&cd=&cad=rja&uact=8&ved=2ahUKewj8xMfA0KmBAXVSr1YBHWIABHAQFnoECB4QAQ&url=https%3A%2F%2Ftitanenviro.com%2Fwp-content%2Fuploads%2F2021%2F05%2FSpartan-Road-Grid-11EPM_March2021.pdf&usg=AOvVaw00i_jFhXVeYb0w6JBme79H&opi=89978449) (accessed on 21 March 2023).
34. Francken, L. Prevention of Cracks in Pavements. *Road Mater. Pavement Des.* **2005**, *6*, 407–425. [CrossRef]
35. Irrometer Irrometer. Available online: <https://www.irrometer.com> (accessed on 21 March 2023).
36. Talebsafa, M.; Romanoschi, S.A.; Papagiannakis, A.T.; Popescu, C. Evaluation of Strains at the Bottom of the Asphalt Base Layer of a Semi-Rigid Pavement Under a Class 6 Vehicle. *MATEC Web Conf.* **2019**, *271*, 08008. [CrossRef]
37. Grellet, D.; Doré, G.; Bilodeau, J.P. Comparative Study on the Impact of Wide Base Tires and Dual Tires on the Strains Occurring within Flexible Pavements Asphalt Concrete Surface Course. *Can. J. Civ. Eng.* **2012**, *39*, 526–535. [CrossRef]

38. Pant, A.; Datta, M.; Ramana, G.V.; Bansal, D. Measurement of Role of Transverse and Longitudinal Members on Pullout Resistance of PET Geogrid. *Measurement* **2019**, *148*, 106944. [[CrossRef](#)]
39. Bhowmik, R.; Shahu, J.T.; Datta, M. Influence of Transverse and Longitudinal Members of Coated Polyester-Yarn Geogrid on Pullout Response Under Low Normal Stress. *Int. J. Civ. Eng.* **2023**, *21*, 33–50. [[CrossRef](#)]

**Disclaimer/Publisher's Note:** The statements, opinions and data contained in all publications are solely those of the individual author(s) and contributor(s) and not of MDPI and/or the editor(s). MDPI and/or the editor(s) disclaim responsibility for any injury to people or property resulting from any ideas, methods, instructions or products referred to in the content.